Maria A. Ponomar[1] [iD], Veronika V. Sarapulova[1*] [iD], Vera V. Guliaeva[1] [iD],
Pavel Yu. Apel[2] [iD], Natalia D. Pismenskaya[1] [iD]

[1]Kuban State University, Krasnodar, Russia;
[2]Joint Institute for Nuclear Research, Dubna, Moscow region, Russia
(*Corresponding author's e-mail: vsarapulova@gmail.com)

Transport Properties of Cation-Exchange Membranes Obtained by Pore Filling of Track-Etched Membranes with Perfluorosulfonic Acid Polymer

In this paper the correlation between the structural characteristics and transport properties of pore-filling membranes formed by embedding an ion-conducting polymer into track-etched substrates was studied. Cation-exchange membranes were fabricated by filling the pores of track-etched membranes with a perfluorosulfonic acid polymer (trade mark LF-4SC). The resulting membranes differed in the volume fraction of the ion-conducting polymer and in the presence or absence of a surface LF-4SC layer. SEM and ATR-FTIR spectroscopy were employed to characterize the chemical composition and structure of the membranes. A comparative analysis of ion-exchange capacity and water uptake was carried out. Concentration dependences of specific electrical conductivity and diffusion permeability in NaCl solutions were obtained. The effects of pore filling degree and LF-4SC layer thickness on osmotic transport, diffusion permeability, and selectivity were analyzed. The electrical resistance of the prepared membranes was found to be comparable to that of the commercial MF-4SC membrane, produced from the same perfluorosulfonic acid polymer, despite a significant fraction of the polymer in the new membranes not participating in counterion transport. The observed structure–property relationships were interpreted within the framework of the two-phase microheterogeneous model, providing insight into the functional behavior of the composite membranes.

Keywords: cation-exchange membranes, track-etched membranes, pore-filling membranes, perfluorosulfonic, electrical conductivity, osmotic flux, diffusion permeability, true transport numbers

1. Introduction

The growing demand for ion-exchange membranes (IEMs) and proton-exchange membranes (PEMs), driven by expanding application areas, has stimulated exponential research efforts. Beyond dialysis and electrodialysis, IEMs and PEMs are now used in a wide range of technologies, including membrane bioreactors, hydrogen production electrolyzers, low-temperature fuel cells, flow batteries, and membrane capacitive deionization, etc. Meeting these diverse requirements demands a careful balance between high transport performance and cost control. Consequently, understanding the relationship between membrane structure and transport properties is essential to address this challenge [1, 2]. The microheterogeneous model, originally formulated by N.P. Gnusin et al. [3, 4] and later refined [5–7], provides a valuable framework for predicting the transport characteristics of ion-exchange membranes. Based on effective medium theory [8], this model describes a swollen IEM (or PEM) as a multiphase system, in which membrane properties are determined by the intrinsic features and spatial organization of the constituent phases. In the simplest case, a membrane is considered as a two-phase system. The first phase, known as the "gel phase", includes the inert binder, reinforcing fabric and the polymer matrix carrying fixed groups, as well as a charged solution of mobile counterions (and, to a lesser extent, coions) that neutralize the charge of the fixed groups. The second phase is an electroneutral solution, identical to the external equilibrium solution, which fills the intergel space, including structural defects and the central regions of meso- and macropores of the IEM (PEM). The microheterogeneous model is mainly employed to interpret the concentration-dependent behavior of several key membrane properties, such as specific electrical conductivity [9–13], diffusion permeability [14–16], and sorption capacity [13, 17–19]. It is also used to determine the volume fractions of the gel phase (f_2) and intergel space (f_1), the coefficient α reflecting the spatial arrangement of the phases, and to estimate counterion and coion diffusion coefficients within the membrane [11, 20]. Most studies applying this model have focused on (1) homogeneous membranes with a uniform nanostructure, (2) quasi-homogeneous composite membranes, or

(3) heterogeneous membranes [21, 22]. Type (1) includes monopolymer or interpolymer membranes, for example, Nafion 117 (DuPont, USA) and CJMA-4 (Hefei Chemjoy Polymer Material Co, China). Quasi-homogeneous (2) composite membranes, such as CSE, ASE (Astom, Japan), consist of an ion-exchange material containing granules of inert binder (40–60 nm). Heterogeneous membranes (3), for example, Ralex AMH PES (Mega, Czech Republic) and MK-40 (Shchekinoazot, Russia), contain ion-exchange resin granules (5–50 μm) dispersed in an inert binder. Most of these membranes include a reinforcing fabric with a fiber diameter of 30–55 μm [23, 24]. Recently, a new class of quasi-homogeneous membranes, known as pore-filling membranes (PFMs), has been developed. Functional PFMs are attracting increasing attention because their production costs are comparable to those of heterogeneous membranes. This advantage arises from a simpler fabrication process, the use of inexpensive substrates, and lower consumption of pore-filling electrolyte. At the same time, PFMs demonstrate excellent electrochemical characteristics and physicochemical properties similar to those of homogeneous membranes [25–27]. PFMs are typically prepared either by casting an ion-exchange polymer dispersion onto a porous substrate or by soaking the substrate in an ion-exchange polyelectrolyte [22]. Depending on pore orientation within the substrate, PFMs can be classified as isotropic, anisotropic, or asymmetric [28, 29]. Figure 1 illustrates examples of such substrates and a schematic of pores filled with ion-exchange material.
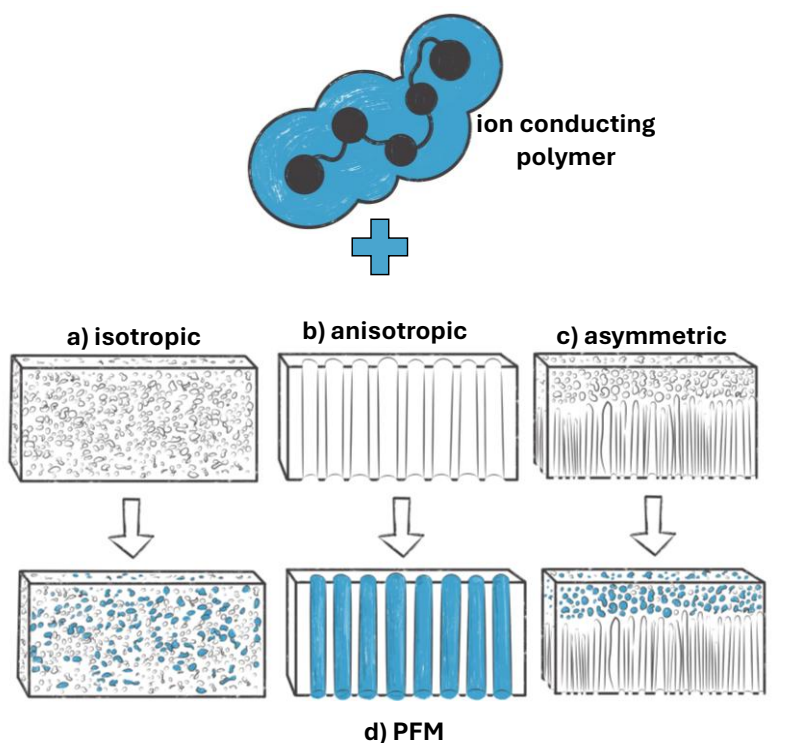

Figure 1. Representative cross-sections of isotropic (*a*), anisotropic (*b*), and asymmetric (*c*) substrates, and PFM (*d*) derived from them

In fact, PFMs combine the advantages of homogeneous ion-exchange films and porous membranes, while their unique structure helps overcome traditional challenges such as the compromise between thickness and mechanical stability, as well as high ion-exchange capacity and water uptake [30]. The morphology of the porous substrate provides high mechanical stability even for relatively thin PFMs and suppresses undesirable excessive swelling of polyelectrolytes in the membrane pores when humidity, temperature, or external solution concentration changes [31]. A substantial reduction in the number of dead-end pores, compared to membranes of previous generations, ensures high conductivity of PFMs [32]. A dispersion of perfluorosulfonic acid (PFSA) polymer in various solvents [28, 33–36] and 2-acrylamido-2-methyl-1-propanesulfonic acid (AMPS) [37, 38] are often used as cation-exchange pore-filling agents. Literature sources have also reported the possibility of producing environmentally friendly pore filling membranes [27, 39, 40]. In addition, the pore-filling method is the most common approach for preparing so-called "stimuli-responsive" or "smart" membranes [40–44]. Such membranes not only exhibit good selectivity but may also

possess a range of additional functions. For example, R. Xie et al. fabricated thermo-sensitive membranes by grafting poly(N-isopropylacrylamide) (PNIPAM) onto the surfaces and into the pores of polycarbonate track-etched (PCTE) membranes via plasma-graft pore-filling polymerization [44]. R. Childs et al. [43] prepared pH-sensitive pore-filled membranes by incorporating a cross-linked poly(4-vinylpyridine) gel as the pore-filling electrolyte into a porous polyethylene host membrane; in this case, the pure-water permeability of the resulting membrane was reversibly controlled by pH. Commercial examples of PFMs include membranes from Fujifilm Manufacturing B.V. (The Netherlands), which use a nonwoven polyolefin porous substrate made of polyolefin fibers [45], as well as the Nafion™ XL membrane by Ion Power Inc. (USA), which employs a woven microporous substrate made of expanded polytetrafluoroethylene [33].

Anisotropic materials, in particular track-etched membranes (TMs), show considerable promise as PFM substrates due to their ordered, parallel and through pores oriented perpendicular to the membrane surface plane, as well as their regular pore geometry with a narrow pore size distribution (Fig. 1*b*). Several studies [46, 47] have demonstrated that PFMs with TM substrates exhibit enhanced electrical conductivity compared to conventional IEMs (PEMs), which is attributed to the reduced tortuosity of the counterion transport pathways. Moreover, the low thickness and high mechanical strength of TMs indicate the potential for reduced surface resistance in TM-based PFMs. Despite the growing number of publications on PFMs with TM substrates [28, 34, 48–50], a significant gap remains in the literature regarding the relationship between structure and transport characteristics of these membranes, particularly when analyzed using modern modeling approaches such as the microheterogeneous model.

This study aims to elucidate the relationship between structure and transport properties of pore-filling membranes prepared by incorporating an ion-conducting polymer into track-etched substrates. The specific objectives are: (i) experimental determination of key structural parameters; (ii) measurement of specific electrical conductivity, diffusion permeability, and counterion/coion transport numbers; and (iii) interpretation of the structure–transport property relationship using the two-phase microheterogeneous model.

2. Experimental

2.1 Membranes

Track-etched membranes with different pore diameters and pore densities were used to fabricate cation-exchange PFMs (Table 1). The TMs were produced at the Flerov Laboratory of Nuclear Reactions, Joint Institute for Nuclear Research (Dubna, Russia) from polyethylene terephthalate films (Hostaphan RNK, Mitsubishi Polyester Films, Japan). The methodology and details of the TM fabrication process are reported elsewhere [51]. The structural, transport, and electrochemical properties of TM 24 and TM 543 have been described previously [52]. A dispersion of LF-4SC (OJSC Plastpolymer, Russia) in the H^+ form (10 % in isopropyl alcohol, equivalent weight — average weight of the polymer per functional group — 980 g mol^{-1}) was used as a cation-exchange filler. LF-4SC is obtained by radical copolymerization of tetrafluoroethylene and fluorovinyl ether with a fluorosulfone group [53].

T a b l e 1

Some characteristics of TM used as anisotropic substrates for PFMs fabrication

Parameter	TM-24	TM-543	TM-120
Matrix material	polyethylene terephthalate		
Fixed groups	-COOH, -OH		
[1]Pore diameter, d_p, nm	1340 ± 10	580 ± 5	140 ± 3
[1]Surface pore density, N×10[7] cm^{-2}	1	7	89
[2]Surface porosity, ε %	12 ± 1	19 ± 1	14 ± 1
[1] — the number of tracks (pores) per unit area was estimated using SEM images;			
[2] — total pore area normalized per unit area of the membrane surface; estimated using the equation $\varepsilon = (1/4)\pi N d_p^2$ [54].			

All TM substrates were initially weighed in an air-dry state and subsequently cleaned by sequential washing with isopropanol (C_3H_8O, 99.9 %, Sigma-Aldrich) and deionized water (conductivity = 5.28 ± ± 0.01 μS cm^{-1}, pH = 4.86 ± 0.01 at 25 °C) prior to any modification.

A track-etched membrane was mounted in a filter holder (vacuum filtration device, Fig. S1, Supplementary Materials) on top of a 1 cm thick silicone rubber band with ~5 μm diameter holes. Ten milliliters of LF-4SC solution (PFSA concentration of 5.0, 2.5, or 1.5 wt %) were applied onto the upper surface of the TM

(Surface 1), and the system was hermetically sealed. Air beneath the membrane was evacuated using a vacuum pump until the first drops of the pore-filling solution appeared at the lower surface of the TM (Surface 2). The sample was then carefully removed and dried in a vacuum oven at 80 °C for 3 hours. This procedure was repeated twice. The resulting membranes were designated PF-Y_X, where Y denotes the track-etched membrane number (Table 1) and X corresponds to the LF-4SC mass concentration in the pore-filling solution.

The commercial homogeneous cation-exchange membrane MF-4SC (OJSC Plastpolymer, Russia) was investigated as a reference for comparative analysis. The membrane MF-4SC (an analogue of Nafion-117) is prepared by solution casting of LF-4SC in the lithium form (10 wt% in dimethylformamide solution).

For conditioning of PFSA-based CEMs, oxidative-thermal pretreatment is commonly employed [47, 55], which removes residual unreacted monomers and leads to pore expansion. In order to avoid possible deformation of the substrate, a standard salt pretreatment [21] was applied to both experimental and commercial membranes in this study.

2.2 Experimental Methods for Membrane Characterization

Morphology of membrane surfaces and cross-sections. The morphology of the membrane surfaces and cross-sections of dry samples was examined after transport characterization using a JEOL JSM-7500F scanning electron microscope (SEM) (JEOL Ltd., Japan). To improve conductivity and enhance image quality, the samples were coated with a thin (about 5 nm) layer of silver nanoparticles. The surface porosity was determined as the ratio of the pore outlet area to the unit area of the TM.

The chemical composition of the surface of air-dried samples was analyzed by energy-dispersive X-ray spectroscopy coupled with SEM, as well as by attenuated total reflectance Fourier-transform infrared (ATR-FTIR) spectroscopy using a Vertex70 spectrometer (Bruker Optics, Germany) in the range of 4000–500 cm^{-1}. The IR spectra were processed using OPUS™ software.

Membrane thickness was measured at least 20 times at different points across each air-dried sample using a Micron MKC-25 digital micrometer (Micron, China). The average thickness and measurement error were then calculated.

Perfluorosulfonic acid polymer content in PF-Y_X. The amount of cation-exchange material in the fabricated membranes (Δm, g cm^{-2}) was calculated as:

$$\Delta m = \frac{m_0 - m_1}{S_0} \times 100 \text{ \%},\tag{1}$$

where m_0 is the weight of the dry track-etched substrate membrane, g; m_1 is the weight of the dry PF-Y_X membrane, g; and S_0 is the membrane area, cm^2.

Water uptake. All membranes were pre-equilibrated in deionized water. The sample was then removed, and excess surface moisture was carefully blotted with filter paper. Subsequently, the sample was placed in an MB25 moisture content analyzer (Ohaus Co., USA). The mass of the swollen sample, m_{sw}, was measured at a temperature of 25 °C. Water was evaporated at 100 °C until a constant mass of the dry sample, m$_{dry}$, was achieved. The water uptake of the membrane, W (%), was calculated as:

$$W = \frac{m_{sw} - m_{dry}}{m_{dry}} \times 100 \text{ \%}.\tag{2}$$

The total ion-exchange capacity (Q) of both strongly acidic cation-exchange membranes and weakly acidic track-etched membranes was determined using the static method [19, 52]. A membrane sample of known dry mass (m_{dry}), converted to the H$^+$ form, was immersed for 24 h with periodic shaking in either 100 mL of 0.1 M sodium hydroxide (for membranes with strongly acidic groups) or 20 mL of 0.01 M sodium acetate (for membranes with weakly acidic groups). The resulting solutions (with the membranes still immersed) were then potentiometrically titrated with 0.1 M HCl solution (strongly acidic fixed groups) or 0.01 M NaOH solution (weakly acidic fixed groups) using an EasyPlusTitrators autotitrator (METTLER TOLEDO, Switzerland). Titration data were recorded via computer output.

The ion-exchange capacity of the dry membrane (strongly acidic fixed groups), Q (mmol g^{-1}) was determined using the formula:

$$Q = \frac{100 - kV}{10 \cdot m_{dry}},\tag{3}$$

where V is the volume of hydrochloric acid solution used for titration; k is a coefficient equal to the ratio of the working solution volume to the aliquot volume.

The calculation of the ion-exchange capacity of the dry membrane (weakly acidic fixed groups) in mmol g^{-1} was carried out according to the equation:

$$Q = \frac{(V_T C_T)}{m_{dry}},$$
(4)

where V_T is the volume of titrant (NaOH) corresponding to the inflection point of the potentiometric titration curve.

Specific electrical conductivity was measured by the difference method [56] using a clip cell and a GW Instek LCR-76002 RLC immittance analyzer (GW Instek, China) in NaCl solutions of 0.1, 0.2, 0.3, 0.4, and 0.5 M.

Diffusion permeability. Integral diffusion permeability coefficients were determined in a two-chamber flow cell according to the procedure described in [19]. The membrane separated compartment I (initially deionized water) and compartment II (NaCl solution: 0.1, 0.2, 0.3, 0.4, 0.5 M). The NaCl concentration in compartment I (C_I) was calculated from electrical conductivity and pH using Kirchhoff's law and the second Gluckauf approximation. The electrolyte diffusion flux density through the membranes was determined as

$J_{dif} = \frac{1}{S}\frac{d(C_I V_I)}{dt}$, where V_I is the volume of water in compartment I and S is the active membrane area.

Osmotic permeability [57] was estimated in conjunction with diffusion permeability by measuring water transfer from compartment I (deionized water) to compartment II (NaCl solution) over 3 hours. The water flux density, J_w [mol s^{-1} m^{-2}], was then calculated using the formula:

$$J_w = \frac{\rho(V_0 - V_t)}{MtS},$$
(5)

where V is the volume of water in compartment I (cm^3), ρ is the density of distilled water (considered equal to 1.0 g cm^{-3}); M is the molar mass of water (18 g mol^{-1}), S is the active area of the swollen membrane (m^2); t is the experiment duration (s). Index 0 denotes the volume in compartment I before the start of the experiment.

Experiments were conducted at 25.0 ± 0.5 °C.

3. Results and Discussion

3.1 Microstructure and Chemical Composition of the Studied Membranes

SEM Images of Dry Samples

Figures 2 and 3 present the surface and cross-section images of both the TM substrates and the resulting PF-Y_X samples.

As seen in Figure 2 and Figure 3, the pore outlets are randomly distributed across the surface of the TM substrates, which is typical of such membranes [58]. SEM cross-sectional images reveal predominantly cylindrical pores (> 0.5 μm) oriented perpendicular to the surface plane. It has been reported [47] that smaller pores exhibit less regular geometries.

Figure 2 and Figure 3 also demonstrate that, in PF-Y_1.5 samples prepared with a pore-filling solution containing 1.5 wt % LF-4SC, the ion-conducting polymer occupies the pores of the TM substrate to a greater extent compared to other cases. The cross-sectional images of PF-Y_1.5 (Fig. 2 b, e, h) clearly show penetration of the LF-4SC polymer into the TM substrate from Surface I, onto which the solution was applied during fabrication. The polymer penetration depth increases in the order PF-120_1.5 < PF-543_1.5 < PF-24_1.5, correlating with the increasing pore diameter of the TM substrate.

When the concentration of LF-4SC in the pore-filling solution was increased, a distinct polymer surface layer formed (as illustrated in Fig. 2 c, f, i). This layer was primarily observed on Surface I, the surface onto which the pore-filling solution had been applied. By contrast, Surface II, which faced the vacuum chamber during the membrane fabrication process, showed only negligible polymer deposition. For example, in the PF-120_X membrane (Fig. 3), Surface I appeared practically homogeneous, whereas the morphology of Surface II remained similar to that of the original TM-120 substrate (Fig. 2c). The thickness of the LF-4SC layer increased in the order PF-24_5 < PF-543_5 < PF-120_5 (Fig. 3, Table 3), indicating an inverse correlation between the thickness of the polymer layer and the pore diameter of the TM substrate.

For comparison, the homogeneous MF-4SC membrane exhibited a uniform surface and bulk structure [59].
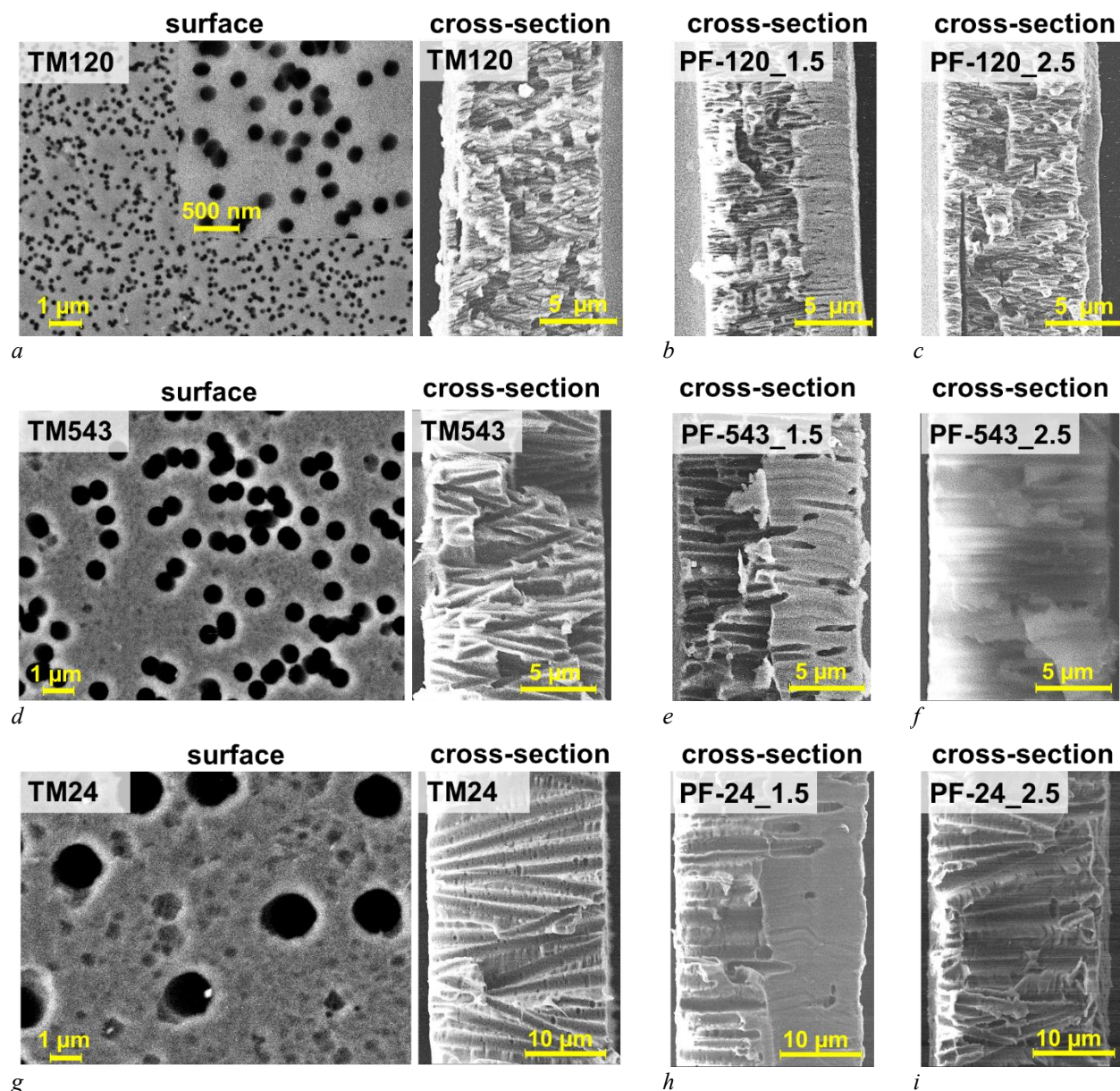
Figure 2. SEM images of the surfaces and cross-sections of the TM substrates (*a, d, g*),
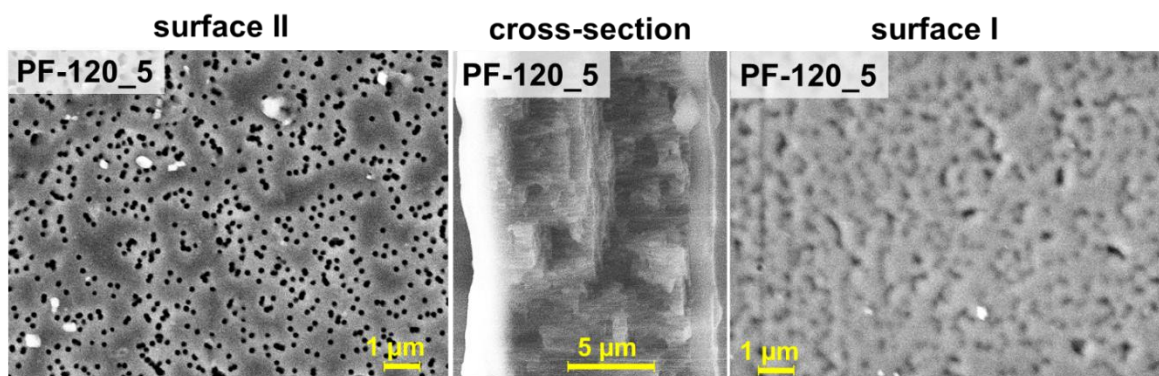as well as cross-sections of the experimental samples PF-Y_1.5 (*b, e, h*) and PF-Y_2.5 (*c, f, i*)

Figure 3. SEM images of the surfaces and cross-section of the experimental sample PF-120_5.
Further details are provided in the text

3.2 Results of ATIR Spectroscopy and Energy-Dispersive X-Ray Spectroscopy

The data obtained from scanning electron microscopy are consistent with the compositional analysis provided by energy-dispersive X-ray (EDX) spectroscopy (Fig. S2, Supplementary Materials), as detailed in Table 2. The EDX results show that on Surface I the fluorine content (originating from the LF-4SC polymer) increases both with higher LF-4SC concentration in the pore-filling solution and with decreasing pore diameter of the substrate surface. In contrast, at Surface II, a higher fluorine content was detected in sample PF-543-2.5 than in PF-120-5.0, suggesting a different trend.

T a b l e 2

Carbon, oxygen and fluorine content (atomic %) on the membrane surface and cross-section

Membrane	$^2\Delta m_{dry}$, mg·cm^{-2}	Surface I			Cross-section (near surface II)		
		C	O	F	C	O	F
TM-Y	–	88	12	–	88	12	–
PF-543 2.5	0.26	55	23	22	63	23	14
PF-120 5.0	0.27	40	2	58	76	21	3
[1]Reproducibility of three measurements is ±2 %. [2]Membrane mass gain after modification.							

Figure 4 shows the IR spectra of the LF-4SC film, the TM-120 track membrane, and the PF-120_5 sample.
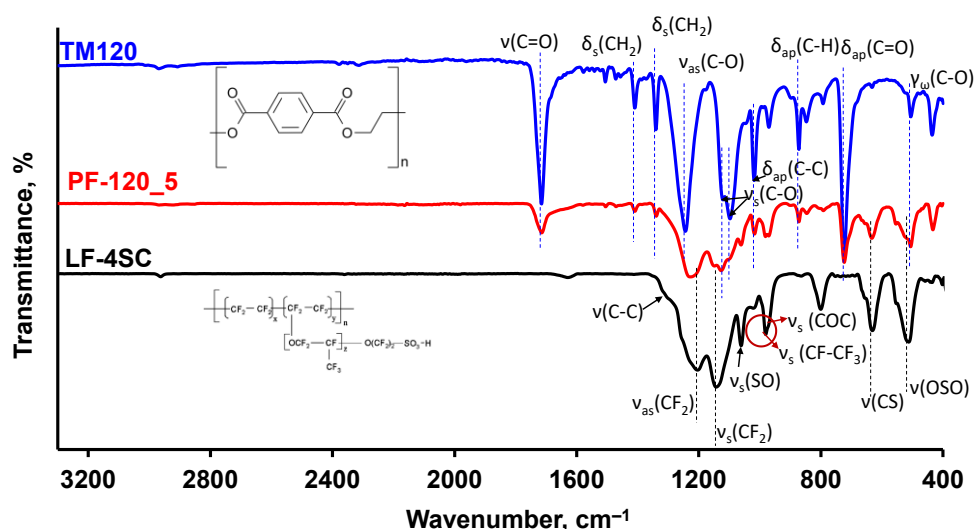

Figure 4. IR spectra of the TM-120 substrate surface, PF-120_5.0 sample cross-section, and LF-4SC film (cast from isopropyl alcohol)

The IR spectrum of the TM-120 substrate exhibits characteristic bands of polyethylene terephthalate [60, 61]: C=O (stretching vibrations of carbonyl groups, 1715 cm^{-1}), C–O (stretching vibrations in ester groups, 1243 cm^{-1}), C–O–C (stretching vibrations in ethers, 1097 cm^{-1} and 1120 cm^{-1}), CH$_2$- (symmetrical bending vibrations of methylene groups in the plane of H atoms, 1410 cm^{-1} and 1340 cm^{-1}), C–C (bending vibrations of the benzene ring in the plane of the ring, 1018 cm^{-1}), C–H (bending vibrations of the benzene ring perpendicular to the plane of the ring, 872 cm^{-1}), C=O (bending vibrations of the carbonyl group in the plane of the C atoms, 723 cm^{-1}).

The IR spectrum of the LF-4SC layer is characterized by asymmetric and symmetric stretching vibrations of the CF$_2$ groups at 1143 and 1203 cm^{-1}, as well as strong stretching of the −SO$_2$F side chain at 1205 cm^{-1} and medium-intensity stretching of the C−O−C group at 989 cm^{-1}, which are characteristic of perfluorsulfonic acid [62, 63]. The IR spectrum of the PF-120_5 sample cross-section is a superposition of the spectra of TM-120 and the LF-4SC film. For PF-120_5, a pronounced decrease in the intensity of the peaks characterizing polyethylene terephthalate is observed, while broad intense peaks appear at 507 cm^{-1},

632 cm^{-1}, along with a weak band at 1060 cm^{-1}, corresponding to symmetric and asymmetric vibrations of sulfo-groups [63].

3.3 Equilibrium and Transport Characteristics of Membranes

Table 3 provides a summary of the key characteristics of the studied membranes. Figure 5 compares area resistance, osmotic water flux (J_w), and NaCl diffusion flux (J_s) for the track-etched membranes and the resulting ion-exchange membranes (PF-Y_X), with MF-4SC included as a reference. The performance of the PF-Y_X membranes is largely governed by the properties of the TM substrates employed in their fabrication (Tables 1, 3).

Table 3

Some characteristics of the membranes under study

Membrane	Δm_{dry}, mg cm^{-2}	d_{sw}, μm	d_{dry}, μm	Δd_{dry}, μm	Q, mmol g$^{-1}_{dry}$	$\Delta Q/\varepsilon$, mmol g$^{-1}_{dry}$	W, %	$\Delta W/\varepsilon$, %
MF-4SC	–	195±2	177±3		0.84	–	24.0	–
TM 24	–	21±1			0.01	–	2.5	–
PF-24_1.5	0.05	23.4	21.0	0.2	0.02	0.09	3.1	5.2
PF-24_2.5	0.06	23.8	22.8	0.8	0.03	0.18	3.4	7.6
PF-24_5	0.17	23.8	23.0	1.0	0.05	0.37	5.0	20.8
TM 543	–	11±1			0.02	–	3.9	–
PF-543_1.5	0.06	12.8	11.7	0.7	0.04	0.08	8.3	23.0
PF-543_2.5	0.26	18.4	15.7	4.7	0.20	0.93	9.5	29.6
PF-543_5	0.45	20.8	19.0	8.0	0.35	1.71	23.4	102.4
TM 120	–	10±1		–	0.05	–	2	–
PF-120_1.5	0.08	14.7	12.8	2.8	0.09	0.31	8.3	45.2
PF-120_2.5	0.12	19.4	16.3	6.3	0.11	0.47	6.1	29.0
PF-120_5	0.27	20.6	18.7	9.5	0.27	1.61	14.9	91.9
Error		±0.05	±0.3		±0.01		±1.0	

Literature [6, 64, 65] reports the formation of a "loose" or "gel layer" on the TM pore walls, containing –OH and –COOH groups. This nanometer-thick layer is generated during heavy ion bombardment followed by chemical etching, as a result of incomplete polymer degradation. The gel layer, typically a few nanometers thick, exhibits ion-exchange characteristics and is capable of swelling in aqueous environments. Polytetrafluoroethylene track-etched membranes have shown surface charge densities ranging from 0.1 to 1 elementary charge per nm², as determined by various methods [6, 64, 65]. Consequently, the ion-exchange capacity of the TMs increases in the following order: TM 24 < TM 543 < TM 120, which correlates with a decreasing pore diameter and increasing pore density (Tables 1 and 3), thereby enhancing the relative contribution of the "gel layer".

The water uptake of TMs depends not only on the degree of hydration of the fixed groups within the gel layer, but also on the amount of free water in the membranes, which is determined by the value of the volume porosity (here assumed to be equivalent to the surface porosity; Table 1). Accordingly, water uptake increases in the order TM 120≈TM 24<TM 543.

The adopted pore-filling strategy for producing PF-Y_X membranes leads to a systematic increase in several key properties with increasing LF-4SC concentration in the impregnating solution. Specifically, increases are observed in the specific mass of the ion-conducting polymer, membrane thickness, ion-exchange capacity, and water uptake (Table 3). The difference in thickness, measured in the dry state, between the PF-Y_X membranes and their corresponding TM substrates allows estimation of the thickness of the LF-4SC layer formed on the surface of these experimental membranes. The lowest values of this parameter (Δd) are observed for PF-Y_1.5 samples (prepared with the 1.5 wt% LF-4SC solution), whereas the highest are found for PF-543_5.0 and PF-120_5.0.

When the ion-conducting polymer is predominantly located within the pores of the PF-Y_X samples, the resulting increase in ion-exchange capacity and water uptake, normalized to the porosity of the TM substrate, shows a relatively weak dependence on the LF-4SC concentration used for pore filling. In contrast, the formation of an LF-4SC film on the surface of the PF-Y_5 samples (fabricated with the highest LF-4SC concentration) leads to a sharp and significant increase in the measured values of ion-exchange capacity ($\Delta Q/\varepsilon$)

and water uptake ($\Delta W/\varepsilon$), as summarized in Table 3. Moreover, when the ion-conducting polymer is primarily located within the pores of the membranes, the rigid and inflexible structure of the TM substrate restricts the swelling of the PF-Y_X samples. However, the particular type of TM substrate used does not appear to exert any significant effect on the degree of swelling exhibited by the LF-4SC surface layer of these membranes.

The observed differences in the extent to which the pores are filled with the ion-exchange material, coupled with the presence of layers of ion-conducting polymer on the surface of certain PF-Y_X samples, give rise to a complex and intricate relationship between the underlying structural parameters of the TM substrate, the concentration of LF-4SC used in the pore filling solution, and the resulting transport characteristics of the fabricated experimental membranes (Fig. 5).
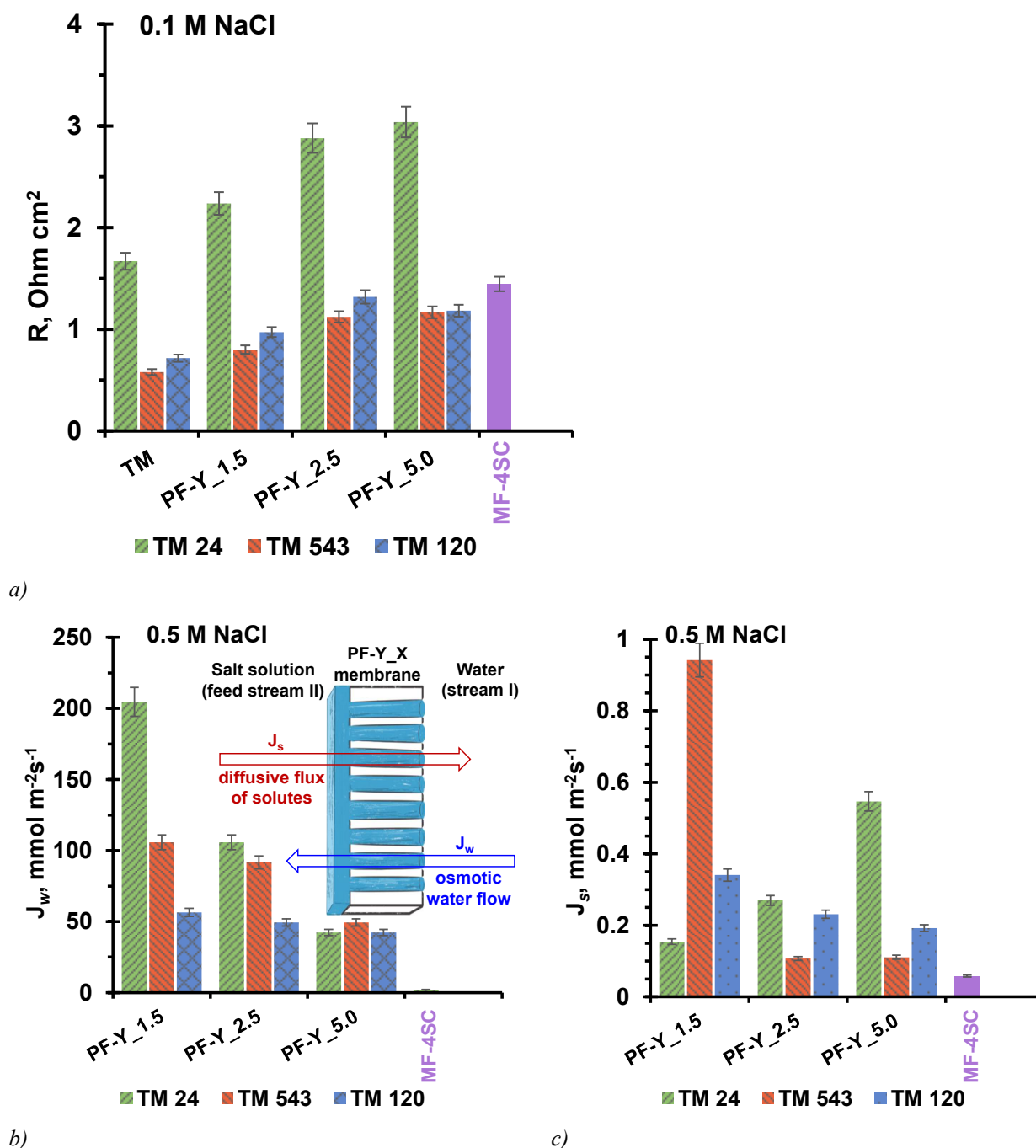

a)

b)   *c)*

Figure 5. Area resistance (*a*), densities of the osmotic water flux J_w (*b*) and electrolyte diffusion flux across the membrane J_s (NaCl) (*c*) of the TM substrates and ion-exchange membranes (PF-Y_X). The characteristics of the MF-4SC membrane are given for comparison

The PF-Y_X membranes exhibit higher area resistance compared to the TM substrates (Fig. 5a), as expected [2]. This effect arises because the ion-exchange material replaces the 0.1 M NaCl solution (90.9 Ohm cm²) within the TM pores, the resistance of which is approximately 1.4 times lower than that of LF-4SC. Furthermore, the LF-4SC film itself adds to the resistance of the PF-Y_X membranes, with the contribution increasing proportionally to its thickness.

Figure 6. Schematic illustration of the PF-Y_X sample, consisting of a layer of LF-4SC
ion-conducting material and a track membrane with straight pores filled with the same ion-conducting material

In line with the concepts outlined in studies [47, 66], the resistance of the PF-Y_X samples, schematically illustrated in Figure 6, can be regarded as the sum of the resistances of the LF-4SC layer and the track-etched membrane, the pores of which are filled with the same ion-exchange material:

$$R_{PF-Y\_X} = R_{FL} + R_{PFL}. \tag{6}$$

Hereafter, the following indices are used: PF-Y_X — a sample of the PFM membrane; FL — the film layer of the LF-4SC polymer on the PFM surface; PFL (pore-filled layer) — the TM with pores filled with the LF-4SC polymer. The resistance of LF-4SC film can be easily estimated using the following formula:

$$R_{FL} = \frac{d_{FL}}{\kappa^*_{FL}}, \tag{7}$$

where κ^*_{FL} is equal to specific electrical conductivity of the LF-4SC. Then:

$$R^{exp}_{PFL} = R^{exp}_{PF-Y\_X} - \frac{d_{FL}}{\kappa^*_{FL}}. \tag{8}$$

The index *exp* denotes the resistance found experimentally.

The resistance of an ideal PFL layer can be estimated under the following assumptions: all pores of the track membrane are straight, and the LF-4SC polymer completely and defect-free fills these pores (Fig. 6). In this case, the PFL can be considered as a parallel circuit consisting of alternating components of the dielectric material of the TM and the ion-exchange material. Accordingly, the resistance of the PFL layer is determined as:

$$\frac{1}{R_{PFL}} = \frac{1}{R_{TM}} + \frac{1}{R_F} \tag{9}$$

Here R_{TM} denotes the resistance of the material from which the track-etched membranes are made. As a first approximation, we may assume that $R_{TM} \to \infty$. Then $R_{PFL} = R_F$, where R_F is the resistance of the LF-4SC polymer, completely filling the pores:

$$R_{PFL} = R_F = \frac{d_{PFL}}{\varepsilon \kappa^*_{FL}}, \tag{10}$$

where ε is the volume fraction of pores in the PFL layer, which is equal to the volumetric porosity of the TM. To estimate the value of R^{exp}_{PFL}, we use equation (10), substituting ε^{exp} in place of ε. The parameter ε^{exp} accounts for the incomplete filling of TM pores with the LF-4SC polymer. The coefficient γ is determined as follows:

$$\gamma\left(\%\right)=100\frac{R_{PFL}^{exp}-R_{PFL}}{R_{PFL}}=100\frac{\varepsilon-\varepsilon^{exp}}{\varepsilon^{exp}}, \tag{11}$$

allows estimation of the proportion of TM pores that are not filled with the LF-4SC polymer.

The estimated γ values, calculated using formula (11), are presented in Figure 7. These values correlate well with the SEM morphological observations, indicating that a decrease in TM pore diameter and an increase in LF-4SC concentration in the pore-filling solution both enhance the fraction of pore volume left unoccupied by the LF-4SC polymer. Notably, despite this incomplete filling, the R values measured for the PF-543_X and PF-120_X samples are comparable to those obtained for the MF-4SC membrane (Fig. 5a). This result, favorable for electromembrane applications, is primarily attributed to the markedly reduced thickness of PFMs relative to conventional membranes.

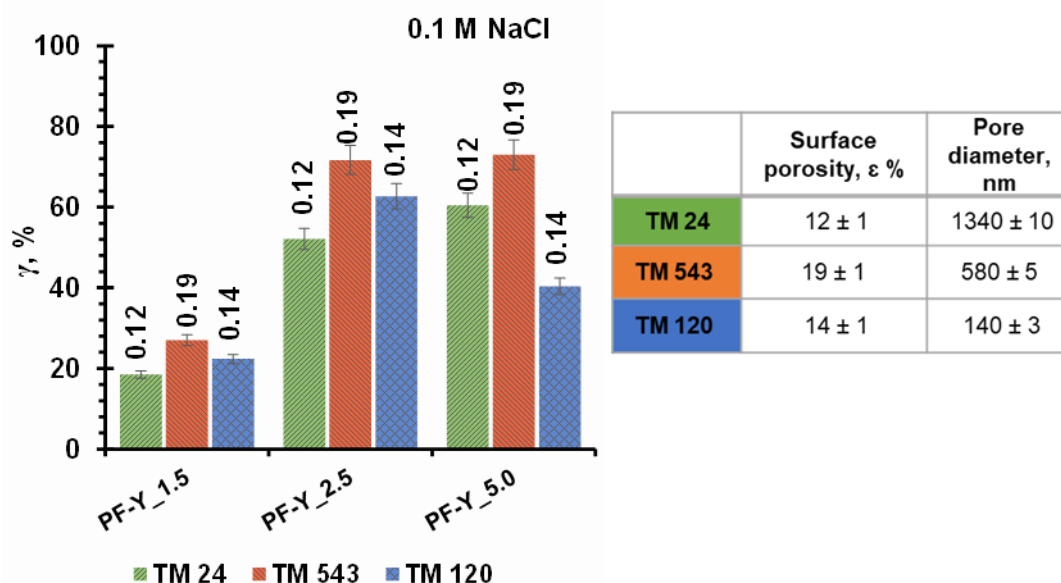|	Surface porosity, ε %	Pore diameter, nm
TM 24	12 ± 1	1340 ± 10
TM 543	19 ± 1	580 ± 5
TM 120	14 ± 1	140 ± 3

Figure 7. Proportion of PF-Y_X pores not filled with LF-4SC ion-conducting polymer.
The surface porosity (assumed to be equal to the volume porosity) for each TM is provided in the table

Due to the fact that the thickness of the electrical double layer formed on the pore walls is two orders of magnitude smaller than the pore diameter (Table 1) [6], water transport through the TM membrane can occur even under a small pressure difference. In contrast, the PF-Y_X samples lose this ability because of pore filling (Fig. 3c). Moreover, the measured values of J_w (osmotic water flux) decrease with increasing LF-4SC concentration in the pore-filling solution and with increasing thickness of the LF-4SC layer formed on the PF-Y_X surface. Despite this decrease in J_w, the resulting values still significantly exceed those that are measured for the MF-4SC membrane. The comparatively high J_w values can be attributed to non-uniform pore filling with the ion-exchange material, a defect that is most apparent in the PF-24_1.5 sample, but is also present in all of the obtained samples (as can be seen in Fig. 5). The presence of the LF-4SC layer as a continuous film on the surface of the PF-Y_5.0 samples further reduces water flux density. However, these values still remain elevated, primarily because the thickness of this surface film is much smaller than the total thickness of the MF-4SC membrane (Table 3).

The electrolyte diffusion flux through the PF-Y_X experimental membranes is generally higher than that measured for the commercial MF-4SC membrane (Fig. 3d). Notably, for the PF-24_X samples, the flux increases with increasing LF-4SC concentration, whereas for the PF-543_X and PF-120_X samples, the flow decreases with increasing LF-4SC concentration in the pore-filling solution. The largest reductions in diffusion flux, relative to the MF-4SC membrane, are observed for PF-543_2.5 and PF-543_5.0.

The differences in how the TM pore morphology and LF-4SC concentration affect the osmotic and diffusion permeability of the membranes are presumably attributed to the PF-Y_X fabrication process. Due to the amphiphilic nature of the PFSA polymer, it readily forms micelles in polar solvents such as water and isopropyl alcohol [67, 68], which prevents complete, void-free filling of the substrate pores. The effect of polymer aggregation is further enhanced by decreasing the substrate pore size [28, 69] and increasing the

polyelectrolyte concentration in the pore filling solution, which increases its viscosity. Consequently, for each substrate with a specific pore diameter, there exists an optimal polymer concentration that leads to the formation of nanovoids [70]. The presence of these nanovoids introduces a complex influence on both the osmotic pressure (which should be applied to the concentrated solution to prevent the solvent from transferring across the membrane) and the diffusion of electrolyte through the membrane [35, 71]. It is noteworthy that the osmotic and diffusion flows across the membrane are oppositely directed (insertion in Fig. 5b), hence a high osmotic flux can effectively hinder electrolyte diffusion across the membrane.

Considering all the data, the PF-120_5 and PF-543_5 samples emerge as the most suitable for providing an optimized balance between transport characteristics, mechanical strength, minimal membrane thickness, and efficient use of ion-exchange material.

3.4 Structural and Transport Parameters of the Studied Membranes

The two-phase microheterogeneous model [4] provides a deeper understanding of the structure-property relationship in PF-120_5 and PF-543_5 membranes. Using this model, the structural and transport parameters of these membranes, along with those of MF-4SC, were determined from the concentration dependence of their specific conductivity (Fig. 8a, b) and diffusion permeability (Fig. 8c) in NaCl solutions.
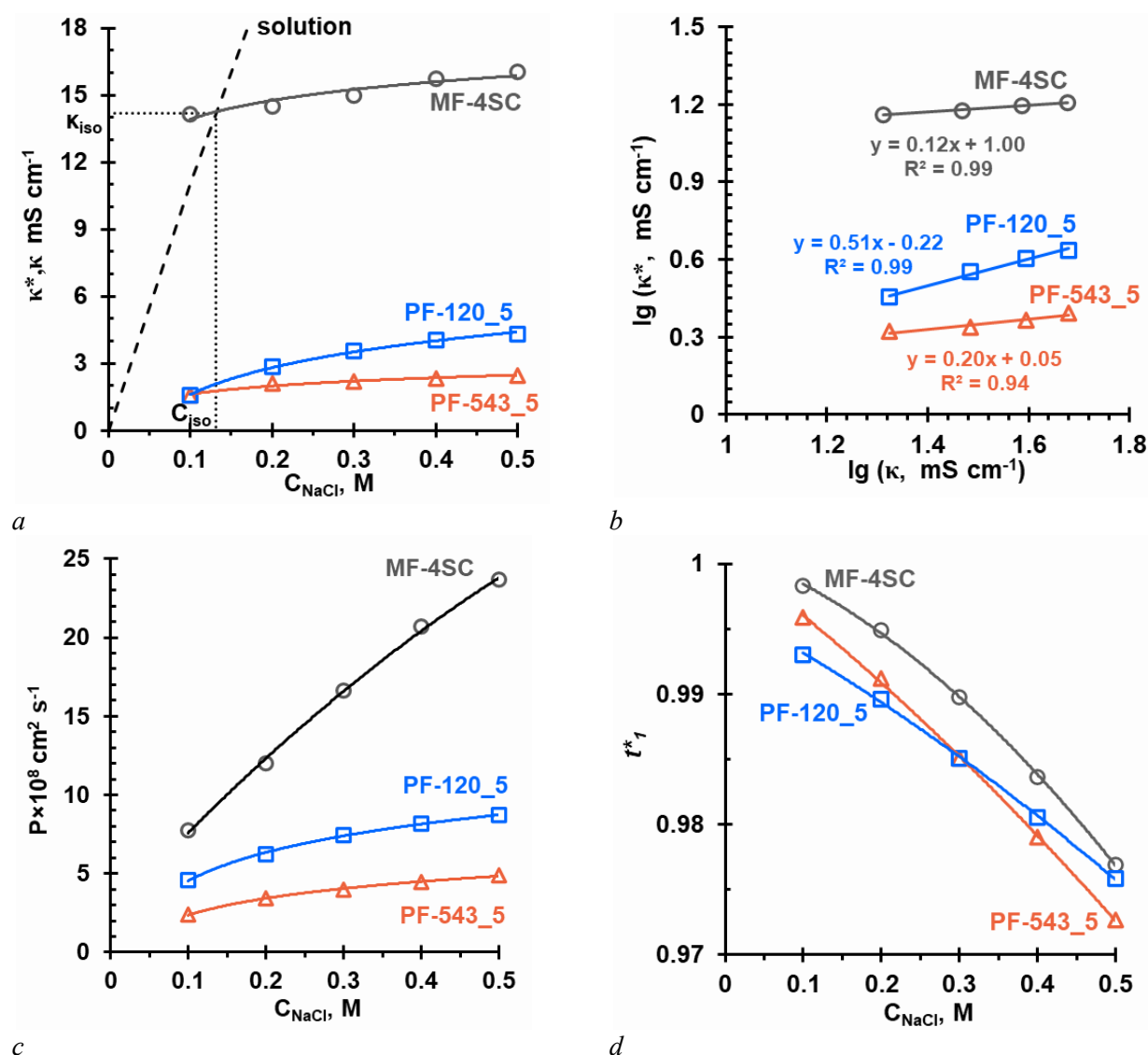

Figure 8. Concentration dependences of specific electrical conductivity κ^* (a), integral coefficient of diffusion permeability P (c) and counterion transport numbers t_1^* (d) of the studied membranes in NaCl solution. Figure (b) demonstrates the procedure for determining the parameter f_2. The numbers near the curves correspond to the membrane designations (Table 3). The dotted line in Fig. (a) corresponds to the concentration dependence of the solution's electrical conductivity

Table 5 presents values of the structural parameter (α, characterizing gel phase/intergel space arrangement), intergel space volume fraction (f_2), ion-exchange capacity ($\bar{Q}$) and counterion diffusion coefficient ($\bar{D}_1$) in the gel phase, as obtained from the microheterogeneous model. Figure 8*b* illustrates the f_2 determination from the slope of membrane electrical conductivity versus NaCl solutions concentration curves (logarithmic coordinates). Details on determining other parameters are provided in [19, 72].

<div align="right">T a b l e 5</div>

Structural and transport parameters of the studied membranes in NaCl solution, determined using a microheterogeneous model

Membrane	f_2	α	$\bar{Q}$, mmol cm^{-3}$_{sw}$	$\bar{D}_1 \times 10^6$, cm^2 s^{-1}
MF-4SC	0.12±0.02	0.35±0.02	1.1±0.1	2.9±0.2
PF-543_5	0.20±0.02	0.27±0.02	0.5±0.1	0.6±0.2
PF-120_5	0.51±0.02	0.09±0.02	0.7±0.1	0.2±0.2

Prior to discussing the data obtained, it should be noted that the studied MF-4SC membrane apparently exhibits lower crystallinity compared to similar membranes reported in [73–75]. This follows from the higher water uptake, specific electrical conductivity, volume fraction of intergel spaces, and the value of the diffusion permeability coefficient of MF-4SC (Figure 8, Table 5), which may result from differences in solvent removal (annealing) conditions during commercial membrane production, as well as variations in pretreatment procedures.

The specific electrical conductivity of the membranes is primarily governed by counterion transport. For the experimental PF-543_5 and PF-120_5 membranes, as well as for the commercial MF-4SC membrane, specific conductivity increases with increasing concentration of the external solution. This behavior is typical of most ion-exchange membranes in strong electrolyte solutions and has been extensively discussed in the literature [24]. Within the studied range of NaCl concentrations, the conductivity of the PF-543_5 and PF-120_5 samples is nearly an order of magnitude lower than that of the commercial MF-4SC membrane (Fig. 8*a*). This reduction, discussed in Section 3.2, is mainly attributed to the low volume fraction of pores in the track-etched membranes and the incomplete filling of these pores with the LF-4SC polymer. Based on the derived f$_2$ values (Table 5), the PF-120_5 sample appears to contain a greater number of voids filled with the external solution than the PF-543_5 sample. As mentioned in Section 3.1, this difference arises from the partial aggregation of the LF-4SC polymer due to its high concentration in the pore-filling solution [28, 69]. However, it is important to note that, only in the case of the MF-4SC membrane, the studied concentration range satisfies the condition $0.1 C_{iso} < C < 10 C_{iso}$, where C_{iso} represents the concentration of isoelectric conductivity of the gel phase and the intergel space. This condition is required for the simplified equation $\kappa^* = \bar{\kappa}^{f_1} \kappa^{f_2}$ to be applicable (the derivation of this equation is provided in the S3, Supplementary materials). Consequently, the f_2 values that were determined for the PF-120_5 and PF-543_5 samples may be overestimated [24].

Parameter α (characterizing gel/intergel phase arrangement) increases in the sequence: PF-120_5 < PF-543_5 < MF-4SC (Table 5). This trend suggests a gradual transition from a predominantly parallel arrangement of these phases in PF-120_5 to a more balanced combination of parallel and sequential contacts in MF-4SC. The primary determinant of the α values appears to be the morphology of the LF-4SC polymer within the pores rather than the thickness of the LF-4SC layer on the surface of the TM substrates (Table 3). Considering the inherent measurement uncertainties, the studied membranes exhibit a clear inverse relationship between α and f_2 (Fig. 9), a behavior commonly observed in many commercial membranes [4, 76, 77].

The ion exchange capacity of the gel phase ($\bar{Q} = Q / f_1$) of the PF-120_5.0 and PF-545_5.0 samples is the same, taking into account the measurement error, and is almost three times lower compared to the same parameter for the commercial MF-4SC membrane. These data also indirectly indicate incomplete filling of the PFL pores with the LF-4SC ion-conducting polymer.

The diffusion coefficient of counterions in the membrane ($\bar{D}_1 \times 10^6$) decreases in the sequence MF-4SC> PF-543_5> PF-543_5, reflecting the increasing pore-filling defects in the PFL layer of the experimental samples.
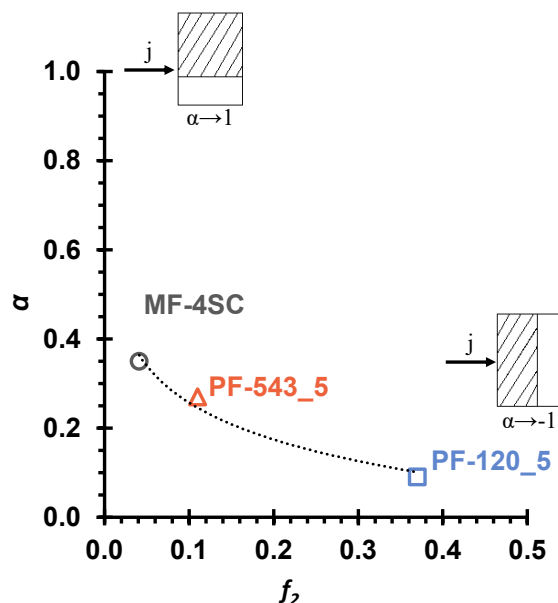
Figure 9. Dependence of the parameter α on the parameter f_2 of the studied membranes in a NaCl solution

The diffusion permeability of membranes is primarily governed by coion transport, effectively representing the non-selective transport of electrolyte through the ion-exchange membrane. Consistent with observations for many other ion-exchange membranes [24], the diffusion permeability of MF-4SC, PF-120_5.0, and PF-545_5.0 increases with increasing concentration of the external solution (Fig. 8c), a phenomenon attributed to the reduced effectiveness of the Donnan (electrostatic) exclusion of coions from the gel phase of the membrane [78]. Somewhat unexpectedly, the slope of these dependencies decreases in the order MF-4SC > PF-120_5.0 > PF-545_5.0. The concentration of coions within the gel phase is, to a first approximation, inversely proportional to the concentration of fixed ions, i.e., the ion-exchange capacity of the gel phase $(\bar{Q} = Q / f_1)$. The higher the density of the fixed groups, the stronger the Donnan exclusion of coions from the gel phase. Consequently, it might be expected that the diffusion permeability of the membrane would decrease with increasing $\bar{Q}$ and with decreasing f_2, as the Donnan exclusion of coions is not effective within the intergel space. On the other hand, if the intergel solution forms a continuous pathway for coion transport, the values of P can be relatively high. This case is most likely to occur with a predominantly parallel arrangement of the f_1 and f_2 phases, which corresponds to α→ −1. However, it appears that the primary factor contributing to the reduced diffusion permeability coefficient of the membranes is not these effects but rather the low overall pore content within the PFL structure, which restricts the available pathways for coion transport.

The transport numbers of coions, t_A and counterions ($t_1^* = 1 - t_A$) were calculated using the equations proposed in [72] (derivation provided in S3, Supplementary Materials) and the experimental concentration dependences of the specific electrical conductivity and diffusion permeability of the studied membranes (Fig. 8). It is known [72] that, to a first approximation, the transport number of counterions determines the membrane selectivity. Its value is proportional to the conductivity and inversely proportional to the diffusion permeability of the membrane. The calculated values (Fig. 8d) indicate that, within the studied NaCl concentration range, the selectivity of the experimental PF-120_5 and PF-543_5 membranes approaches that of the commercial MF-4SC membrane. As mentioned earlier, the higher t_1^* values of the MF-4SC membrane compared to the PF-Y_5.0 membranes are due to the higher $\bar{Q}$ values and the absence of areas of the TM pores not filled with LF-4SC polymer.

Furthermore, physicochemical properties of the fabricated PF-543_5 membrane were evaluated, and a comparison was made with commercially available cation-exchange membranes [38, 79, 80] as well as previously reported laboratory-prepared pore-filling membranes [37–39, 79–82] in terms of key properties, including thickness, IEC, transport number, electrical resistance, and water uptake (Table S1). The values of the "true" (t_1^*) transport number of PF-543_5 membrane prepared in the present study were comparable to

previously reported apparent (t^*_{1app}) counterion transport numbers determined using the potentiometric method [24, 37]. The resistance of PF-543_5 was lower than that of commercial ion-exchange membranes but generally higher than that of PFMs prepared on the basis of an isotropic substrate. The water uptake of the prepared membrane was lower than that of the compared membranes. Both of these factors can be explained by the low porosity of the original track membrane.

4. Conclusions

It is demonstrated that pore filling of the track-etched membrane with the PFSA polymer LF-4SC is an effective approach for producing thin cation-exchange membranes. The best-performing membranes obtained in this study exhibit electrical resistance and selectivity comparable to the commercial MF-4SC membrane, with the added advantage of reduced swelling upon dilution of the external electrolyte solution. However, these same samples show higher osmotic and diffusion fluxes compared to MF-4SC. These performance differences arise from incomplete filling of the track-etched membrane pores with the ion-conducting material, as well as from the formation of the LF-4SC layer on one of the PF-Y_X membrane surfaces. These undesirable trends observed for the transport characteristics of the experimental samples become more pronounced with increasing concentration of LF-4SC (from 1.5 wt % to 5 wt %) in the pore-filling solution and with decreasing pore diameter of the track-etched membranes.

Modeling the PF-Y_X membranes as track-etched membranes with straight pores filled with an ion-conducting polymer, overlaid with a surface layer of the same polymer, allows quantifying the contribution of pore-filling defects to the overall resistance of the samples. Furthermore, analysis of the concentration-dependent data for specific electrical conductivity and integral diffusion permeability coefficients of the PF-Y_X samples using a microheterogeneous model demonstrates that, when these pore-filling defects are taken into account, the fabricated membranes exhibit the same fundamental behaviors characteristic of most commercial ion-exchange membranes.

The set of determined transport characteristics for the PF-543_5 sample (R 0.89 Ohm·cm^2, J_w 49.4 mmol m^{-2} s^{-1}, J_s 0.11 mmol m^{-2} s^{-1}, t$^*_1$ = 0.97 in 0.5M NaCl) indicates its potential suitability for use in electrodialyzer-concentrators and other electromembrane modules.

Supporting Information

The Supporting Information is available free at https://ejc.buketov.edu.kz/index.php/ejc/article/view/309/279

Author Information*

*The authors' names are presented in the following order: First Name, Middle Name and Last Name

Maria Alekseevna Ponomar — Postgraduate Student, Junior Research Fellow, Kuban State University, 149 Stavropolskaya St., 350040, Krasnodar, Russia; e-mail: ponomar.marie@yandex.ru; https://orcid.org/0000-0001-9139-4954

Veronika Vladimirovna Sarapulova (*corresponding author*) — PhD in Electrochemistry, Senior Researcher, Kuban State University, Stavropolskaya St., 149, 350040, Krasnodar, Russia; e-mail: vsarapulova@gmail.com; https://orcid.org/0000-0002-7902-6662

Vera Vladimirovna Guliaeva — Master's Student, Laboratory Assistant, Kuban State University, Stavropolskaya St., 149, 350040, Krasnodar, Russia; e-mail: vera_gulyaeva_2002@mail.ru; https://orcid.org/0009-0002-9370-9432

Pavel Yuryevich Apel — Doctor of Sciences, Professor, Flerov Laboratory of Nuclear Reactions, Joint Institute for Nuclear Research, 141980, Dubna, Moscow Region, Russia; e-mail: apel@jinr.ru; https://orcid.org/0000-0003-1259-163X

Natalia Dmitrievna Pismenskaya — Doctor of Sciences, Professor, Kuban State University, Stavropolskaya St., 149, 350040, Krasnodar, Russia; e-mail: n_pismen@mail.ru; https://orcid.org/0000-0001-5736-0136

Author Contributions

The manuscript was written through contributions of all authors. All authors have given approval to the final version of the manuscript. CRediT: **Maria Alekseevna Ponomar** investigation, data curation, methodology; **Veronika Vladimirovna Sarapulova** conceptualization, data curation, writing-original draft, writing-review & editing, funding acquisition; **Vera Vladimirovna Guliaeva** investigation, data curation, formal analysis; **Pavel Yuryevich Apel** methodology, resources, writing-review & editing; **Natalia Dmitrievna Pismenskaya** supervision, validation, writing-original draft, writing-review & editing.

Acknowledgments

Conflicts of Interest

The authors declare no conflict of interest.

References

1 Nikonenko, V., Nebavsky, A., Mareev, S., Kovalenko, A., Urtenov, M., & Pourcelly, G. (2018). Modelling of ion transport in electromembrane systems: impacts of membrane bulk and surface heterogeneity. *Applied Sciences*, *9*(1), 25. https://doi.org/10.3390/app9010025

2 Stenina, I., Golubenko, D., Nikonenko, V., & Yaroslavtsev, A. (2020). Selectivity of transport processes in ion-exchange membranes: relationship with the structure and methods for its improvement. *International Journal of Molecular Sciences*, *21*(15), 5517. https://doi.org/10.3390/ijms21155517

3 Gnusin, N. P., Berezina, N. P., Kononenko, N. A., & Dyomina, O. A. (2004). Transport structural parameters to characterize ion exchange membranes. *Journal of Membrane Science*, *243*(1–2), 301–310. https://doi.org/10.1016/j.memsci.2004.06.033

4 Zabolotsky, V. I., & Nikonenko, V. V. (1993). Effect of structural membrane inhomogeneity on transport properties. *Journal of Membrane Science*, *79*(2–3), 181–198. https://doi.org/10.1016/0376-7388(93)85115-D

5 Nichka, V. S., Mareev, S. A., Porozhnyy, M. V., Shkirskaya, S. A., Safronova, E. Yu., Pismenskaya, N. D., & Nikonenko, V. V. (2019). Modified microheterogeneous model for describing electrical conductivity of membranes in dilute electrolyte solutions. *Membranes and Membrane Technologies*, *1*(3), 190–199. https://doi.org/10.1134/S2517751619030028

6 Nichka, V. S., Mareev, S. A., Apel, P. Yu., Sabbatovskiy, K. G., Sobolev, V. D., & Nikonenko, V. V. (2022). Modeling the conductivity and diffusion permeability of a track-etched membrane taking into account a loose layer. *Membranes*, *12*(12), 1283. https://doi.org/10.3390/membranes12121283

7 Porozhnyy, M., Huguet, P., Cretin, M., Safronova, E., & Nikonenko, V. (2016). Mathematical modeling of transport properties of proton-exchange membranes containing immobilized nanoparticles. *International Journal of Hydrogen Energy*, *41*(34), 15605–15614. https://doi.org/10.1016/j.ijhydene.2016.06.057

8 Choy, T. C. (2015). *Effective Medium Theory: Principles and Applications*. Oxford University Press.

9 Sedkaoui, Y., Szymczyk, A., Lounici, H., & Arous, O. (2016). A new lateral method for characterizing the electrical conductivity of ion-exchange membranes. *Journal of Membrane Science*, *507*, 34–42. https://doi.org/10.1016/j.memsci.2016.02.003

10 Vyas, P. V, Ray, P., Adhikary, S. K., Shah, B. G., & Rangarajan, R. (2003). Studies of the effect of variation of blend ratio on permselectivity and heterogeneity of ion-exchange membranes. *Journal of Colloid and Interface Science*, *257*, 127–134. https://doi.org/10.1016/S0021-9797(02)00025-5

11 Davydov, D., Nosova, E., Loza, S., Achoh, A., Korzhov, A., Sharafan, M., & Melnikov, S. (2021). Use of the microheterogeneous model to assess the applicability of ion-exchange membranes in the process of generating electricity from a concentration gradient. *Membranes*, *11*(6), 406. https://doi.org/10.3390/membranes11060406

12 Gohil, G. (2004). Comparative studies on electrochemical characterization of homogeneous type of ion-exchange membranes. *Journal of Membrane Science*, *240*(1–2), 211–219. https://doi.org/10.1016/j.memsci.2004.04.022

13 Le, X. T., Bui, T. H., Viel, P., Berthelot, T., & Palacin, S. (2009). On the structure–properties relationship of the AMV anion exchange membrane. *Journal of Membrane Science*, *340*(1–2), 133–140. https://doi.org/10.1016/j.memsci.2009.05.025

14 Loza, N. V, & Kutenko, N. A. (2024). Effect of Nature and Charge of Counterions and Co-Ions on Electrotransport Properties of Heterogeneous Anion Exchange Membranes. *Membranes and Membrane Technologies*, *6*(3), 193–204. https://doi.org/10.1134/S2517751624600274

15 Novikova, S. A., Volodina, E. I., Pis'menskaya, N. D., Veresov, A. G., Stenina, I. A., & Yaroslavtsev, A. B. (2005). Ionic transport in cation-exchange membranes MK-40 modified with zirconium phosphate. *Russian Journal of Electrochemistry*, *41*(10), 1070–1076. https://doi.org/10.1007/s11175-005-0183-z

16 Zabolotskii, V. I., Loza, S. A., & Sharafan, M. V. (2005). Physicochemical properties of profiled heterogeneous ion-exchange membranes. *Russian Journal of Electrochemistry*, *41*(10), 1053–1060. https://doi.org/10.1007/s11175-005-0180-2

17 Tuan, L. X., Verbanck, M., Buess-Herman, C., & Hurwitz, H. D. (2006). Properties of CMV cation exchange membranes in sulfuric acid media. *Journal of Membrane Science*, *284*(1–2), 67–78. https://doi.org/10.1016/j.memsci.2006.06.036

18 Iddya, A., Zarzycki, P., Kingsbury, R., Khor, C. M., Ma, S., Wang, J., Wheeldon, I., Ren, Z. J., Hoek, E. M. V., & Jassby, D. (2022). A reverse-selective ion exchange membrane for the selective transport of phosphates via an outer-sphere complexation–diffusion pathway. *Nature Nanotechnology*, *17*(11), 1222–1228. https://doi.org/10.1038/s41565-022-01209-x

19 Pismenskaya, N. D., Nevakshenova, E. E., & Nikonenko, V. V. (2018). Using a single set of structural and kinetic parameters of the microheterogeneous model to describe the sorption and kinetic properties of ion-exchange membranes. *Petroleum Chemistry*, *58*(6), 465–473. https://doi.org/10.1134/S0965544118060087

20 Salmeron-Sanchez, I., Asenjo-Pascual, J., Avilés-Moreno, J. R., & Ocón, P. (2022). Microstructural description of ion exchange membranes: The effect of PPy-based modification. *Journal of Membrane Science*, *659*, 120771. https://doi.org/10.1016/j.memsci.2022.120771

21 Berezina, N. P., Kononenko, N. A., Dyomina, O. A., & Gnusin, N. P. (2008). Characterization of ion-exchange membrane materials: Properties vs structure. *Advances in Colloid and Interface Science*, *139*(1–2), 3–28. https://doi.org/10.1016/j.cis.2008.01.002

22 Xu, T., & Wang, Y. (2024). *Ion Exchange Membranes: Design, Preparation, and Applications*. Wiley-VCH GmbH.

23 Stránská, E., & Neděla, D. (2018). Reinforcing fabrics as the mechanical support of ion exchange membranes. *Journal of Industrial Textiles*, *48*(2), 432–447. https://doi.org/10.1177/1528083717732075

24 Sarapulova, V., Pismenskaya, N., Titorova, V., Sharafan, M., Wang, Y., Xu, T., Zhang, Y., & Nikonenko, V. (2021). Transport characteristics of CJMAED^{TM} homogeneous anion exchange membranes in sodium chloride and sodium sulfate solutions. *International Journal of Molecular Sciences*, *22*(3), 1415. https://doi.org/10.3390/ijms22031415

25 Eti, M., Hidayati Othman, N., Guuml; ler, E., & Kabay, N. (2021). Ion exchange membranes for reverse electrodialysis RED) applications—Recent developments. *Journal of Membrane Science and Research*, *7*(4). https://doi.org/10.22079/jmsr.2021.534937.1482

26 Niccolai, F., Guazzelli, E., El Koura, Z., Pucher, I., & Martinelli, E. (2025). A critical update on the design of dense ion-conducting membranes for redox flow batteries. *Advanced Sustainable Systems*, *9*(2), 2400661. https://doi.org/10.1002/adsu.202400661

27 Yang, S., Choi, Y. -W., Choi, J., Jeong, N., Kim, H., Jeong, H., Byeon, S. Y., Yoon, H., & Kim, Y. H. (2019). Green fabrication of pore-filling anion exchange membranes using R2R processing. *Journal of Membrane Science*, *584*, 181–190. https://doi.org/10.1016/j.memsci.2019.04.075

28 Gloukhovski, R., Freger, V., & Tsur, Y. (2018). Understanding methods of preparation and characterization of pore-filling polymer composites for proton exchange membranes: A beginner's guide. *Reviews in Chemical Engineering*, *34*(4), 455–479. https://doi.org/10.1515/revce-2016-0065

29 Fan, H., Xu, Y., Zhao, F., Chen, Q. -B., Wang, D., & Wang, J. (2023). A novel porous asymmetric cation exchange membrane with thin selective layer for efficient electrodialysis desalination. *Chemical Engineering Journal*, *472*, 144856. https://doi.org/10.1016/j.cej.2023.144856

30 Wu, J., Dai, Q., Zhang, H., & Li, X. (2020). Recent development in composite membranes for flow batteries. *ChemSusChem*, *13*(15), 3805–3819. https://doi.org/10.1002/cssc.202000633

31 Chavan, V., Agarwal, C., Adya, V. C., & Pandey, A. K. (2018). Hybrid organic-inorganic anion-exchange pore-filled membranes for the recovery of nitric acid from highly acidic aqueous waste streams. *Water Research*, *133*, 87–98. https://doi.org/10.1016/j.watres.2018.01.023

32 Kim, D.-H., Seo, S.-J., Lee, M.-J., Park, J.-S., Moon, S.-H., Kang, Y. S., Choi, Y.-W., & Kang, M.-S. (2014). Pore-filled anion-exchange membranes for non-aqueous redox flow batteries with dual-metal-complex redox shuttles. *Journal of Membrane Science*, *454*, 44–50. https://doi.org/10.1016/j.memsci.2013.11.051

33 Shi, S., Weber, A. Z., & Kusoglu, A. (2016). Structure/property relationship of Nafion XL composite membranes. *Journal of Membrane Science*, *516*, 123–134. https://doi.org/10.1016/j.memsci.2016.06.004

34 Dalal, U., Kapoor, M., & Verma, A. (2023). Low-cost pore-filled PVDF–Nafion composite membrane for the vanadium redox flow battery. *Energy & Fuels*, *37*(17), 13457–13466. https://doi.org/10.1021/acs.energyfuels.3c01932

35 Fang, Y., & Leddy, J. (1995). Surface diffusion in microstructured, ion-exchange matrixes: Nafion/Neutron Track-Etched Polycarbonate Membrane composites. *The Journal of Physical Chemistry*, *99*(16), 6064–6073. https://doi.org/10.1021/j100016a049

36 Kang, S. E., & Lee, C. H. (2015). Perfluorinated sulfonic acid ionomer-PTFE pore-filling membranes for polymer electrolyte membrane fuel cells. *Membrane Journal*, *25*(2), 171–179. https://doi.org/10.14579/MEMBRANE_JOURNAL.2015.25.2.171

37 Cha, J.-E., Seo, M. H., Choi, Y.-W., & Kim, W. B. (2021). A practical approach to measuring the ion-transport number of cation-exchange membranes: Effects of junction potential and analyte concentration. *Journal of Membrane Science*, *635*, 119471. https://doi.org/10.1016/j.memsci.2021.119471

38 Yang, S., Choi, Y.-W., Choi, J., Jeong, N., Kim, H., Nam, J.-Y., & Jeong, H. (2019). R2R fabrication of pore-filling cation-exchange membranes via one-time impregnation and their application in reverse electrodialysis. *ACS Sustainable Chemistry & Engineering*, acssuschemeng.9b01450. https://doi.org/10.1021/acssuschemeng.9b01450

39 Wang, B., Yan, J., Wang, H., Li, R., Fu, R., Jiang, C., Nikonenko, V., Pismenskaya, N., Wang, Y., & Xu, T. (2024). Solvent-free fabrication of pore-filling cation-exchange membranes for highly efficient desalination. *Chemical Engineering Science*, *287*, 119782. https://doi.org/10.1016/j.ces.2024.119782

40 Wang, M., An, Q.-F., Wu, L.-G., Mo, J.-X., & Gao, C.-J. (2007). Preparation of pH-responsive phenolphthalein poly(ether sulfone) membrane by redox-graft pore-filling polymerization technique. *Journal of Membrane Science*, *287*(2), 257–263. https://doi.org/10.1016/j.memsci.2006.10.049

41 Hu, K., & Dickson, J. M. (2007). Development and characterization of poly(vinylidene fluoride)–poly(acrylic acid) pore-filled pH-sensitive membranes. *Journal of Membrane Science*, *301*(1–2), 19–28. https://doi.org/10.1016/j.memsci.2007.05.031

42 Hu, K., & Dickson, J. M. (2008). Modelling of the pore structure variation with pH for pore-filled pH-sensitive poly(vinylidene fluoride)–poly(acrylic acid) membranes. *Journal of Membrane Science*, *321*(2), 162–171. https://doi.org/10.1016/j.memsci.2008.04.046

43 Mika, A. M., Childs, R. F., & Dickson, J. M. (2002). Salt separation and hydrodynamic permeability of a porous membrane filled with pH-sensitive gel. *Journal of Membrane Science*, *206*(1–2), 19–30. https://doi.org/10.1016/S0376-7388(01)00474-4

44 Xie, R., Chu, L.-Y., Chen, W.-M., Xiao, W., Wang, H.-D., & Qu, J.-B. (2005). Characterization of microstructure of poly(N-isopropylacrylamide)-grafted polycarbonate track-etched membranes prepared by plasma-graft pore-filling polymerization. *Journal of Membrane Science*, *258*(1–2), 157–166. https://doi.org/10.1016/j.memsci.2005.03.012

45 Zou, Z., Wu, L., Luo, T., Yan, Z., & Wang, X. (2021). Assessment of anion exchange membrane selectivity with ionic membrane conductivity, revised with Manning's theory or the Kohlrausch's law. *Journal of Membrane Science*, *635*, 119496. https://doi.org/10.1016/j.memsci.2021.119496

46 Golubenko, D. V., Yurova, P. A., Desyatov, A. V., Stenina, I. A., Kosarev, S. A., & Yaroslavtsev, A. B. (2022). Pore filled ion-conducting materials based on track-etched membranes and sulfonated polystyrene. *Membranes and Membrane Technologies*, *4*(6), 398–403. https://doi.org/10.1134/S2517751622060026

47 Gloukhovski, R., Tsur, Y., & Freger, V. (2017). A Nafion-filled polycarbonate track-etched composite membrane with enhanced selectivity for direct methanol fuel cells. *Fuel Cells*, *17*(1), 56–66. https://doi.org/10.1002/fuce.201600154

48 Parmanbek, N., Sütekin, D. S., Barsbay, M., Mashentseva, A. A., Zheltov, D. A., Aimanova, N. A., Jakupova, Z. Ye., & Zdorovets, M. V. (2022). Hybrid PET track-etched membranes grafted by well-defined poly(2-(dimethylamino)ethyl methacrylate) brushes and loaded with silver nanoparticles for the removal of As(III). *Polymers*, *14*(19), 4026. https://doi.org/10.3390/polym14194026

49 Korolkov, I. V., Yeszhanov, A. B., Shakayeva, A. Kh., Shlimas, D. I., Zhumazhanova, A., & Zdorovets, M. V. (2022). Photo-induced graft (co)polymerization of glycidyl methacrylate and acrylonitrile on PET ion-track membranes for electrochemical detection of uranyl ions. *Colloids and Surfaces A: Physicochemical and Engineering Aspects*, *648*, 129086. https://doi.org/10.1016/j.colsurfa.2022.129086

50 Meyer, N., Arroyo, N., Janot, J. -M., Lepoitevin, M., Stevenson, A., Nemeir, I. A., Perrier, V., Bougard, D., Belondrade, M., Cot, D., Bentin, J., Picaud, F., Torrent, J., & Balme, S. (2021). Detection of amyloid-β fibrils using track-etched nanopores: effect of geometry and crowding. *ACS Sensors*, *6*(10), 3733–3743. https://doi.org/10.1021/acssensors.1c01523

51 Hoek, E. M. V., & Tarabara, V. V. (2013). *Encyclopedia of Membrane Science and Technology*. Wiley. https://doi.org/10.1002/9781118522318

52 Sarapulova, V. V., Pasechnaya, E. L., Titorova, V. D., Pismenskaya, N. D., Apel, P. Yu., & Nikonenko, V. V. (2020). Electrochemical properties of ultrafiltration and nanofiltration membranes in solutions of sodium and calcium chloride. *Membranes and Membrane Technologies*, 2(5), 332–350. https://doi.org/10.1134/S2517751620050066

53 Yaroslavcev, A. B., & Nikonenko, V. V. (2009). Ionoobmennye membrannye materialy: svojstva, mo-difikaciya i prakticheskoe primenenie [Ion-exchange membrane materials: properties, modification and practical application]. *Rossiiskie Nanotekhnologii — Russian Nanotechnologies, 4*(3–4), 33–53 [in Russian].

54 Apel, P. Yu., & Dmitriev, S. N. (2004). Optimizaciya formy por trekovyh membrane [Optimization of the pore shape of track membranes]. *Seriya. Kriticheskie Tekhnologii. Membrany — Series. Critical Technologies. Membranes, 3*(23), 32–37 [in Russian].

55 Berezina, N. P., Timofeev, S. V., Rolle, A. L., Fedorovich, N. V., & Dyuran-Vidal', S. (2002). Elektrotransportnye i strukturnye svojstva perftorirovannyh membran Nafion-117 i MF-4SK [Electrotransport and structural properties of perfluorinated membranes Nafion-117 and MF-4SC]. *Elektrohimiya — Electrochemistry*, *38*(8), 1009–1015 [in Russian].

56 Karpenko, L. V., Demina, O. A., Dvorkina, G. A., Parshikov, S. B., Larshe, K., Okler, B., & Berezina, N. P. (2001). Sravnitel'noe izuchenie metodov opredeleniya udel'noj elektroprovodnosti ionoob-mennyh membrane [Comparative study of methods for determining the specific conductivity of ion-exchange membranes]. *Elektrokhimiia — Electrochemistry, 37*(3), 328–335 [in Russian].

57 Galama, A. H., Saakes, M., Bruning, H., Rijnaarts, H. H. M., & Post, J. W. (2014). Seawater predesalination with electrodialysis. *Desalination*, *342*, 61–69. https://doi.org/10.1016/j.desal.2013.07.012

58 Gumirova, V. N., Razumovskaya, I. V., Apel, P. Yu., Bedin, S. A., & Bazhenov, S. L., Abdura-shidova, G. S. (2013). Metody opredeleniya raspredeleniya por po poverhnosti trekovyh membrane [Methods for determining the distribution of pores on the surface of track membranes]. *Prepodavatel' XXI Vek — Teacher XXI Century, 2* [in Russian].

59 Sanchez, C., Espinos, F. J., Barjola, A., Escorihuela, J., & Compañ, V. (2022). Hydrogen production from methanol–water solution and pure water electrolysis using nanocomposite perfluorinated sulfocationic membranes modified by polyaniline. *Polymers*, *14*(21), 4500. https://doi.org/10.3390/polym14214500

60 Kravec, L. I., Yarmolenko, M. A., Rogachev, A. A., Gajnutdinov, R. V., Altynov, V. A., & Lizunov, N. E. (2021). Formirovanie na poverhnosti trekovyh membrangidrofobnyh pokrytij metodom el-ektronno-luchevogo dispergirovaniya polivinilhlorida v vakuume [Formation of hydrophobic mem-brane coatings on the surface of track films using the method of electron beam dispersion of polyvinyl chloride in a vacuum]. *Nanoindustriya Rossii — Nanoindustry of Russia*, *14*(6s), 44–54 [in Russian]. https://doi.org/10.22184/1993-8578.2021.14.6s.44.54

61 Djebara, M., Stoquert, J. P., Abdesselam, M., Muller, D., & Chami, A. C. (2012). FTIR analysis of polyethylene terephthalate irradiated by MeV He+. *Nuclear Instruments and Methods in Physics Research Section B: Beam Interactions with Materials and Atoms*, *274*, 70–77. https://doi.org/10.1016/j.nimb.2011.11.022

62 Liang, Z., Chen, W., Liu, J., Wang, S., Zhou, Z., Li, W., Sun, G., & Xin, Q. (2004). FT-IR study of the microstructure of Nafion® membrane. *Journal of Membrane Science*, *233*(1–2), 39–44. https://doi.org/10.1016/j.memsci.2003.12.008

63 Kinumoto, T., Inaba, M., Nakayama, Y., Ogata, K., Umebayashi, R., Tasaka, A., Iriyama, Y., Abe, T., & Ogumi, Z. (2006). Durability of perfluorinated ionomer membrane against hydrogen peroxide. *Journal of Power Sources*, *158*(2), 1222–1228. https://doi.org/10.1016/j.jpowsour.2005.10.043

64 Déjardin, P., Vasina, E. N., Berezkin, V. V., Sobolev, V. D., & Volkov, V. I. (2005). Streaming potential in cylindrical pores of poly(ethylene terephthalate) track-etched membranes: variation of apparent ζ potential with pore radius. *Langmuir*, *21*(10), 4680–4685. https://doi.org/10.1021/la046913e

65 Apel, P. Yu., Blonskaya, I. V., Ivanov, O. M., Kristavchuk, O. V., Lizunov, N. E., Nechaev, A. N., Orelovich, O. L., Polezhaeva, O. A., & Dmitriev, S. N. (2020). Creation of ion-selective membranes from polyethylene terephthalate films irradiated with heavy ions: critical parameters of the process. *Membranes and Membrane Technologies*, *2*(2), 98–108. https://doi.org/10.1134/S251775162002002X

66 Yaroslavtsev, A. B. (2012). Ion conductivity of composite materials on the base of solid electrolytes and ion-exchange membranes. *Inorganic Materials*, *48*(13), 1193–1209. https://doi.org/10.1134/S0020168512130055

67 Ma, C.-H., Yu, T. L., Lin, H.-L., Huang, Y.-T., Chen, Y.-L., Jeng, U.-S., Lai, Y.-H., & Sun, Y.-S. (2009). Morphology and properties of Nafion membranes prepared by solution casting. *Polymer*, *50*(7), 1764–1777. https://doi.org/10.1016/j.polymer.2009.01.060

68 Safronova, E. Yu., Voropaeva, D. Yu., Safronov, D. V., Stretton, N., Parshina, A. V., & Yaroslavtsev, A. B. (2022). Correlation between Nafion morphology in various dispersion liquids and properties of the cast membranes. *Membranes*, *13*(1), 13. https://doi.org/10.3390/membranes13010013

69 Kim, R., Kim, H. G., Doo, G., Choi, C., Kim, S., Lee, J.-H., Heo, J., Jung, H.-Y., & Kim, H.-T. (2017). Ultrathin Nafion-filled porous membrane for zinc/bromine redox flow batteries. *Scientific Reports*, *7*(1), 10503. https://doi.org/10.1038/s41598-017-10850-9

70 Khandavalli, S., Park, J. H., Winter, H. H., Myers, D. J., Ulsh, M., & Mauger, S. A. (2023). Viscoelasticity enhancement and shear thickening of perfluorinated sulfonic acid ionomer dispersions in water–alcohol solvent mixtures. *Macromolecules*, *56*(17), 6988–7005. https://doi.org/10.1021/acs.macromol.3c00383

71 Yamauchi, Y., Blonskaya, I. V., & Apel', P. Yu. (2019). Osmos v otricatel'no zaryazhennyh nanoka-pil-lyarah i ego usilenie anionnym poverhnosto-aktivnym veshchestvom [Osmosis in negatively charged nanocapillaries and its enhancement by cationic surfactant]. *Kolloidnyj Zhurnal — Colloid Journal*, *81*(1), 125–136 [in Russian]. https://doi.org/10.1134/S0023291219010166

72 Larchet, C., Dammak, L., Auclair, B., Parchikov, S., & Nikonenko, V. (2004). A simplified procedure for ion-exchange membrane characterisation. *New Journal of Chemistry*, *28*(10), 1260. https://doi.org/10.1039/b316725a

73 Kusoglu, A., & Weber, A. Z. (2017). New insights into perfluorinated sulfonic-acid ionomers. *Chemical Reviews*, *117*(3), 987–1104. https://doi.org/10.1021/acs.chemrev.6b00159

74 Yin, C., Wang, Z., Luo, Y., Li, J., Zhou, Y., Zhang, X., Zhang, H., Fang, P., & He, C. (2018). Thermal annealing on free volumes, crystallinity and proton conductivity of Nafion membranes. *Journal of Physics and Chemistry of Solids*, *120*, 71–78. https://doi.org/10.1016/j.jpcs.2018.04.028

75 Kamel, M. S. A., Mohamed, H. F. M., Abdel-Hamed, M. O., & Abdel-Hady, E. E. (2019). Characterization and evaluation of Nafion HP JP as proton exchange membrane: Transport properties, nanostructure, morphology, and cell performance. *Journal of Solid State Electrochemistry*, *23*(9), 2639–2656. https://doi.org/10.1007/s10008-019-04366-7

76 Salmeron-Sanchez, I., Asenjo-Pascual, J., Avilés-Moreno, J. R., Pérez-Flores, J. C., Mauleón, P., & Ocón, P. (2022). Chemical physics insight of PPy-based modified ion exchange membranes: A fundamental approach. *Journal of Membrane Science*, *643*, 120020. https://doi.org/10.1016/j.memsci.2021.120020

77 Falina, I. V., Demina, O. A., Kononenko, N. A., & Annikova, L. A. (2017). Influence of inert components on the formation of conducting channels in ion-exchange membranes. *Journal of Solid State Electrochemistry*, *21*(3), 767–775. https://doi.org/10.1007/s10008-016-3415-0

78 Luo, T., Abdu, S., & Wessling, M. (2018). Selectivity of ion exchange membranes: A review. *Journal of Membrane Science*, *555*, 429–454. https://doi.org/10.1016/j.memsci.2018.03.051

79 Kim, D.-H., Choi, Y.-E., Park, J.-S., & Kang, M.-S. (2019). Capacitive deionization employing pore-filled cation-exchange membranes for energy-efficient removal of multivalent cations. *Electrochimica Acta*, *295*, 164–172. https://doi.org/10.1016/j.electacta.2018.10.124

80 Kim, D.-H., & Kang, M.-S. (2018). Water electrolysis using pore-filled proton-exchange membranes for hydrogen water production. *Chemistry Letters*, *47*(10), 1265–1268. https://doi.org/10.1246/cl.180560

81 Akter, M., & Park, J. -S. (2023). Fouling and mitigation behavior of foulants on ion exchange membranes with surface property in reverse electrodialysis. *Membranes*, *13*(1), 106. https://doi.org/10.3390/membranes13010106

82 Fan, H., Xu, Y., Zhao, F., Chen, Q. -B., Wang, D., & Wang, J. (2023). A novel porous asymmetric cation exchange membrane with thin selective layer for efficient electrodialysis desalination. *Chemical Engineering Journal*, *472*, 144856. https://doi.org/10.1016/j.cej.2023.144856